Journal of Engineering Technology and Applied Physics

Utilisation of Response Surface Methodology to Optimise Bandgap and Resistance of Nickel Oxide using The Sol-gel Method

Nurbahirah Norddin[1, 2, 4, *], Suhaidi Shafie[2, 3], Muhammad Idzdihar Idris[1], Xinzhi Liu[2, 3], Ismail Lawal[2, 3] and Mohd Nizar Hamidon[2, 3]

[1]*Faculty of Electronics and Computer Technology and Engineering, Technical University of Malaysia Melaka (UTeM), 75450 Melaka, Malaysia.*

[2]*Department of Electrical and Electronic Engineering, Faculty of Engineering, Universiti Putra Malaysia, 43400 Serdang, Selangor, Malaysia.*

[3]*Institute of Nanoscience and Nanotechnology, Universiti Putra Malaysia, 43400 Serdang, Selangor, Malaysia.*

[4]*Faculty of Electrical Technology and Engineering, Technical University of Malaysia Melaka (UTeM), 75450 Melaka, Malaysia.*

[*]*Corresponding author*: nurbahirah@utem.edu.my, *ORCiD*: 0000-0002-4687-1413

https://doi.org/10.33093/jetap.2026.8.2.5

Manuscript Received: 18 August 2025, Revised: 14 November 2025, Accepted: 20 December 2025, Published: 15 September 2026

***Abstract*—Nickel oxide (NiO) is a promising hole transport layer for inverted perovskite solar cells, but its bandgap and resistance are highly sensitive to synthesis conditions. This study applies Response Surface Methodology to optimize precursor molarity, solution pH, and annealing temperature for NiO thin films prepared via the sol–gel method. The optimal condition 0.125 M, pH 10, and 450 °C yielded a bandgap of 3.6 eV and low electrical resistance, suitable for efficient hole transport. These results demonstrate that annealing temperature and pH significantly influence NiO properties, enabling reproducible fabrication of high-performance films.**

***Keywords*—Sol gel, Nickel Oxide, Optimization, Box Behnken, Perovskite.**

I. INTRODUCTION

Perovskite solar cells (PSCs) are promising photovoltaic technologies due to high efficiencies, tunable bandgaps, low-temperature processing, and flexible substrate compatibility. The inverted (p–i–n) architecture is popular for easy fabrication, less hysteresis, and better stability [1]. The hole transport layer (HTL) is key, allowing efficient hole extraction and transport while preventing electron recombination.

Nickel oxide (NiO) draws attention as an inorganic HTL for inverted PSCs for its thermal stability, wide bandgap, deep valence band, and good energy match with perovskite absorbers [2]. It offers better environmental stability than organic HTLs such as Spiro-OMeTAD [3] or PEDOT: PSS [4]. Despite these advantages, the optoelectronic performance of NiO thin films made by sol-gel depends heavily on processing, especially electrical resistance and optical bandgap, which affect charge carrier behaviour [5]. Deviations from optimal properties can negatively impact device efficiency and stability.

A primary challenge is to achieve both an optimal bandgap (~3.6 eV) for valence band alignment and low electrical resistance for efficient hole extraction. Synthesis parameters precursor concentration, solution pH, and annealing temperature significantly affect the structure and electronics of nickel oxide (NiO) films. Therefore, systematically optimizing these parameters is essential for producing consistently high-quality NiO layers for PSC applications. A bandgap of about 3.6 eV is optimal, as shown by previous studies. This paper identifies ~3.6 eV as the best NiO bandgap for several reasons. First, it aligns the NiO valence band (about 5.4 eV) with the perovskite absorber (see Fig.1), promoting efficient hole extraction and reducing recombination at the interface [6]. Secondly, a relatively wide bandgap (~3.6 eV) makes nickel oxide (NiO) transparent to visible light, allowing photons to pass through efficiently to the perovskite layer, thus maximizing photon absorption and ultimately enhancing photocurrent. Additionally, by positioning the conduction band of nickel oxide (NiO) significantly

Published by MMU PRESS. URL: https://journals.mmupress.com/index.php/jetap/index

higher than the conduction band of the perovskite, electron recombination is minimized [7], directly leading to higher open-circuit voltages and improved fill factors. A hole transport layer exhibiting low resistivity is characterized by a high intrinsic carrier concentration, efficient hole mobility, and minimized charge recombination losses.

In this research, we utilize Response Surface Methodology (RSM) based on a Box–Behnken design to statistically analyse and optimise the influence of three key sol-gel synthesis parameters: nickel acetate tetrahydrate molarity, solution pH, and annealing temperature. By focusing on the optical bandgap and sheet resistance as primary response variables, we aim to develop a predictive model that reduces experimental effort while enabling precise control over nickel Oxide (NiO) properties. This approach promotes reproducibility, scalability, and cost-effective fabrication of durable, high-performance perovskite solar cells.

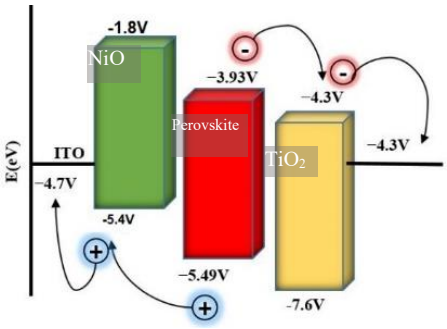

Fig. 1. The energy level diagram.

II. METHODOLOGY

A. Experimental Procedure

Glass is cut into 1.5 cm × 2.0 cm pieces with a cutter and cleaned with tap water and detergent. It is soaked in distilled water for 10 minutes, then placed in an ultrasonic cleaner. Next, it is soaked in acetone for 10 minutes and ultrasonicated, then treated the same way with isopropyl alcohol for 10 minutes. Three concentrations of NiO thin film precursor are made by dissolving 0.311 g, 0.778 g, and 1.244 g of nickel acetate tetrahydrate (Ni(OCOCH3)2·4H2O) in ethanol (15 ml) and isopropyl alcohol (10 ml) to get final concentrations of 0.05 M, 0.125 M, and 0.2 M.

Next, 0.56 g of potassium hydroxide (KOH) was added to 100 ml of deionized water at room temperature. The mixture was added dropwise to adjust the solution pH to 9, 10 or 11. After raising the temperature to 60ºC, the solution pH was recorded. When left overnight at room temperature, the solution separated into two layers, with precipitate settling at the bottom. The solution was centrifuged with JoanLab to separate heavier from lighter particles quickly by applying high rotational forces. This method achieves faster isolation than gravity alone. Spin coating was done at 3000 rpm for 15 seconds for pristine nickel oxide (NiO). The thin film was then annealed at 300ºC, 500ºC or 700ºC for 1 hour.

B. Response Surface Method (RSM)

Response Surface Methodology is a set of mathematical techniques used to evaluate the effects of several factors and find optimal conditions which Box–Behnken Design is a type of experimental design used for this purpose. It is based on fitting a second-order polynomial Eq. (1) to experimental data.

$$Y = \beta_0 + \sum_{j=1}^{k} \beta_j X_j + \sum_{j=1}^{k} \beta_{jj} X_j^2 + \sum_{i} \sum_{<j=2}^{k} \beta_{ij} X_i X_j + e_i \quad (1)$$

, where Y is the response (bandgap or resistance), X_i are coded independent variables (precursor concentration, annealing temperature, and solution pH). Then, β terms represent regression coefficients for linear, quadratic, and interaction effects. This model captures curvature and interactions between factors, which are essential for predicting optimal conditions. The Box-Behnken design (BBD) is well-suited for this experiment, which aims to optimize the bandgap and resistance of NiO thin films based on three input parameters: precursor concentration (A, M), annealing temperature (B, ºC), and solution pH (C). Box-Behnken Design (BBD) is beneficial since it accurately captures the effects and interactions between the components while exploring the quadratic response surfaces with fewer experimental runs, which saves time and resources. In contrast to Central Composite Design (CCD) [8], Box-Behnken Design (BBD) avoids extreme values at the corners of the experimental space, hence mitigating the danger of adverse reactions or instability during the film formation process, which is essential for dependable thin-film synthesis [9]. Overall, BBD's focus on midpoints and interaction effects, along with its resource efficiency, makes it ideal for systematically tuning nickel oxide (NiO) film properties to achieve targeted electrical and optical responses. The experimental design was generated using Design-Expert software (version 13), consisting of 17 experimental runs, including three replicates at the centre point to evaluate experimental error and model adequacy. Each independent variable was varied at three levels: low (–1), center (0), and high (+1), as detailed in Table I. This design was selected due to its efficiency in fitting second-order models without requiring a full factorial experiment, thereby reducing the number of experimental trials.

Table I. Factors and levels in the design of Box-Behnken experiments.

Factors	**Levels**		
Nickel acetate concentration (A) / Molar	0.05	0.125	0.2
Annealing temperature (B) / °C	300	500	700
Solution pH (C)	9	10	11

C. Characterization using UV VIS and XRD

Optical absorbance was measured using a Shimadzu 1800 UV-Vis-NIR Spectrometer, and the bandgap was then calculated from the Tauc plot, a graphical method for determining the optical bandgap from absorbance data. UV-vis absorption of NiO samples was analysed to determine their optical bandgap. The energy bandgap was subsequently calculated using the Tauc plot relation, as shown in Eq. (2).

$$(\alpha h\nu)^{1/n} = A(h\nu - E_g) \quad (2)$$

, where α, A, h, ν, n (=1/2 for direct bandgap) and E_g are optical absorption coefficient, absorbance, Planck's constant, frequency of light, a constant related to the mode of transition, and bandgap energy. The bandgap was determined by extrapolating the linear segment of the Tauc plot of $(\alpha h\nu)^2$ versus (eV) to the energy axis intercept.

The X-Ray diffraction measurements to identify crystal structure and crystalline size were performed on samples using (Rigaku Miniflex) with λ=1.54A and an angle of incident ranging from 20º to 90º. The crystallite size in Eq. (3) for the prepared NiO was estimated by taking the crystalline size of the calculated intense peaks at 37.249º, 43.276º, and 62.879º using the Debye-Scherrer equation [10].

$$D = \frac{K\lambda}{\beta cos\theta} \quad (3)$$

D. Characterization using a Linear Four-point Probe

The electrical analysis was performed using a linear four-point probe with a Keithley 2450 as source measure unit and four probe points from Suzhou Jingge Electronics. Linear four-point probe illustration shown in Fig. 2. The thickness of the thin nickel oxide film when using 3000 rpm for 15s will be 600 nm or 0.6μm [11]. The sheet resistance was calculated using Eq. (4), resistivity using Eq. (5) and conductivity using Eq. (6).

$$\rho_{\square}\left(\frac{\Omega}{\square}\right) = \frac{\pi}{ln(2)}\frac{V}{I} = 4.5324\frac{V}{I}[\Omega.\square] \quad (4)$$

$$\rho = \rho_{\square} t \quad (5)$$

$$\sigma = \frac{1}{\rho} \quad (6)$$

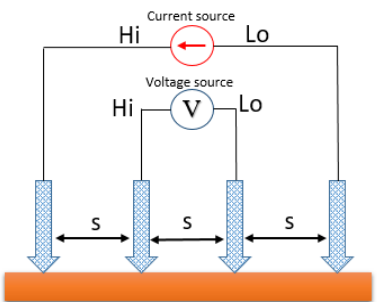

Fig. 2. Linear Four-point Probe.

III. RESULTS AND DISCUSSION

A. Optical and Structural Analysis

The Tauc plot calculated using optical absorbance for different anneal temperatures was calculated using Tauc plot as in Eq. (1) and plotted in Fig. 3. At 300°C, the NiO thin film with 0.125 M pH 11 has a lower bandgap at 3.566 eV. In contrast, the 0.2 M pH 11 sample shows the highest bandgap at 3.862 eV. At 500°C, the NiO thin film with 0.125 M pH 10 shows the highest bandgap (3.675 eV), which is observed for the same 0.125 M pH 10 sample, indicating that the bandgap increases under these specific conditions, likely due to enhanced crystallinity and reduced defect levels. At 700°C, the 0.125 M pH 11 NiO film exhibits the largest bandgap (3.570 eV), as indicated in the graphs.

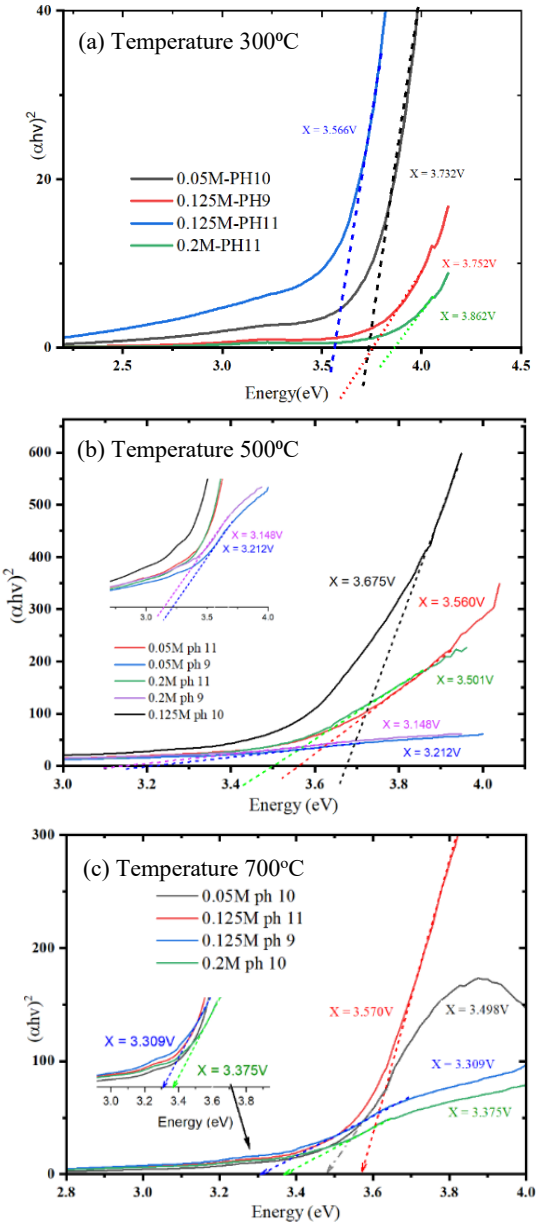

Fig. 3. Tauc plot for different anneal temperatures (a) 300ºC, (b) 700ºC and (c) 700ºC.

X-ray diffraction (XRD) is a widely used methodology for determining the crystallographic structure of materials. The process commences with the application of incident X-rays onto a sample, followed by the measurement of the intensities and scattering angles of the X-rays that emerge from the material. The positions of the atoms in the lattice planes were used to evaluate the intensities and scattering angles. The XRD graph for nickel oxide shows the crystalline type of material shown in Fig. 4. The diffraction peaks at 37.249º, 43.276º, and 62.879º correspond to (111), (200), and (220) planes. Two minor peaks at 75.416º, and 79.409º, are related to (311) and (222) planes. These results are in agreement with the reference JCPDS card no. 47–1049 [12, 13].

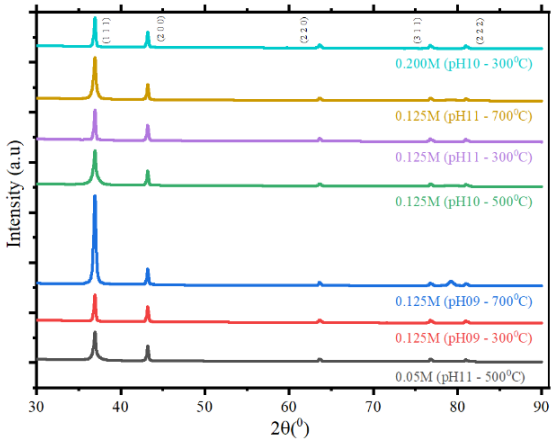

Fig. 4. XRD synthesized NiO at different pH and temperature.

The crystallite size was found to increase as the temperature of annealing increased [14]. The crystallite size increases as the precursor molarity is raised [15]. The observed variations in crystallite size with pH and annealing temperature in 0.125 M nickel oxide (NiO) films synthesized via the sol-gel method can be attributed to the interplay of nucleation and growth kinetics during film formation, as similarly reported in previous studies [12]. At pH 9 and 300°C, the relatively lower crystallite size at size 10.01 nm suggests a dominance of nucleation over growth, likely due to limited thermal energy and moderate ion dissociation, resulting in smaller crystalline domains. Increasing the annealing temperature to 700°C at the same pH promotes enhanced thermal diffusion and recrystallization, allowing for larger crystallites to form due to increased atomic mobility and grain combination. Similarly, raising the pH to 11 at 300°C increases the OH^- concentration, which influences precursor hydrolysis and condensation reactions, leading to a higher degree of super saturation which increase crystallite size at 20.62nm. The combined effect of pH and temperature highlights their critical role in tuning the crystallinity and microstructural properties of NiO films.

B. Electrical Characterization

The electrical performance of NiO-based hole transport layers (HTLs) was evaluated using a four-point probe method shown in Table II, with results indicating a strong dependence on precursor molarity, solution pH, and annealing temperature. Among the investigated samples, the film synthesized using 0.125 M nickel acetate at pH 10 and annealed at 500°C exhibited the lowest resistivity (2.00 Ω·cm) and highest conductivity (0.499 S/cm). The value of conductivity suggests that this particular synthesis condition is optimal for promoting efficient charge transport within the film [16]. In contrast, samples annealed at higher temperatures (700°C), particularly those at pH 09 and pH 11, showed a significant increase in resistivity (over 90 Ω·cm) and a drastic reduction in conductivity (≈ 0.01 S/cm), indicating that excessive thermal exposure may lead to contrary effects on the film's structural or electronic properties. The correlation between improved crystallinity and enhanced electrical conductivity is evident in this sample, as larger crystallite domains reduce grain boundary scattering and dislocation sites that typically trap carriers. In contrast, the samples with smaller crystallite sizes and higher dislocation densities, particularly those processed at 700°C, showed diminished electrical performance, likely due to increased defect states and microstructural stress. These findings collectively indicate that a moderate annealing temperature of 500°C, combined with a pH-optimized precursor solution, facilitates the development of high-quality NiO films with favorable electrical and crystallographic characteristics suited for optoelectronic applications such as perovskite solar cells.

Table II. Measurement obtained from the Linear Four-point Probe.

HTL	Resistance (MΩ)	Sheet Resistance (MΩ/□)	Resistivity (Ω.cm)	Conductivity (σ)
0.125M pH09 300ºC	1.71	1.283	7.7	0.13
0.125M pH11 300ºC	0.841	0.631	3.78	0.264
0.200M pH10 300ºC	0.873	0.655	3.93	0.255
0.050M pH11 500ºC	1.03	0.773	4.64	0.216
0.125M pH10 500ºC	0.4445	0.334	2	0.499
0.125M pH09 700ºC	21.2	15.9	95.4	0.0105
0.125M pH11 700ºC	20.8	15.6	93.6	0.0107

C. Optimization using Response Surface Methodology

In this study, Response Surface Methodology (RSM) based on the Box-Behnken Design (BBD) was applied to evaluate and optimize the synthesis parameters affecting the optical and electrical properties of nickel oxide (NiO) thin films. Three independent variables were selected: nickel acetate concentration (A), annealing temperature (B), and

solution pH (C), each tested at three levels. The resulting responses measured were the optical bandgap (V) and electrical resistance (Ω) of the films. A total of 17 experimental runs were conducted, as summarized in Table III. These data were then analysed using Design Expert software to generate regression models, perform ANOVA, and determine the optimal conditions for achieving the desired material properties. The precursor concentration (molarity), solution pH, and annealing temperature parameters were chosen based on the review of literature findings where such factors have been reported to notably influence the structural, optical, and electrical properties of NiO thin films [17]. The changes in precursor concentration would affect the particle size and morphology of NiO. At a molarity of 0.125 M, the smallest crystalline size is observed at pH 9 and 300 °C. However, at the same pH of 9 but a higher temperature of 700 °C, the crystalline size increases. Additionally, at the same molarity (0.125 M), increasing the pH to 11 at 300 °C also increases the crystalline size. A p-value indicates that an observed effect occurred by chance; values below 0.05 are considered statistically significant, while values below 0.0001 are highly significant, meaning the factor strongly influences the response and the probability of the effect being random is less than 0.01%.

Table III. RSM BBD for bandgap and resistance for nickel oxide (NiO).

Factor A	Factor B	Factor C	Response 1	Response 2
0.125	700	11	3.6	2.08E+07
0.2	500	11	3.501	622000
0.125	500	10	3.501	478000
0.05	700	10	3.498	2.21E+07
0.125	500	10	3.648	518000
0.2	700	10	3.375	2.06E+07
0.125	300	9	3.797	1.71E+06
0.125	700	9	3.309	2.12E+07
0.125	300	11	3.728	841000
0.125	500	10	3.406	445000
0.05	500	11	3.56	1.03E+06
0.2	300	10	3.862	873000
0.05	300	10	3.813	1.63E+06
0.05	500	9	3.212	1.63E+06
0.2	500	9	3.148	935000
0.125	500	10	3.7	817000
0.125	500	10	3.501	456000

D. The Influence of All Parameters on The Bandgap

The influence of three process parameters, nickel acetate tetrahydrate concentration (A), annealing temperature (B), and solution pH (C), on the optical bandgap of NiO thin films was investigated using a Box-Behnken design. In Design Expert software, ANOVA results shown in Table 4 confirmed that the quadratic model was statistically significant ($p = 0.0216$), indicating that the model adequately represents the experimental data. Among the individual terms, annealing temperature (B) ($p = 0.0032$) and solution pH (C) ($p = 0.0242$) were found to have a significant effect on the bandgap. Conversely, nickel acetate concentration (A) showed no significant influence ($p = 0.5605$), suggesting its minimal role within the investigated range. These findings suggest that fine-tuning of annealing temperature and solution pH plays a critical role in modifying the bandgap of NiO. At the same time, precursor concentration may be less influential within the tested levels.

Table IV. Anova result for bandgap.

Source	p-value	Remark
Model	0.0216	significant ($p < 0.05$)
A-concentration	0.5605	not significant ($p > 0.05$)
B-temperature	0.0032	significant ($p < 0.05$)
C-ph	0.0242	significant ($p < 0.05$)

As highlighted in [10], the pH level during the synthesis of nickel oxide (NiO) plays a significant role in influencing its bandgap. Figure 5 shows the 3D plot of bandgap versus temperature versus concentrations while the pH is maintained. Higher pH levels (greater than 10) may result in the creation of structural defects, including oxygen vacancies and nickel, which lead to a reduction in the bandgap and a decrease in resistance due to an augmented concentration of charge carriers. In contrast, diminished pH levels (less than 10) are associated with a reduced presence of defects, enhanced crystallinity, and an expanded bandgap. Yet, this condition also leads to an increase in resistance attributed to a lower density of charge carriers and a more compact film morphology.

(a) PH 9

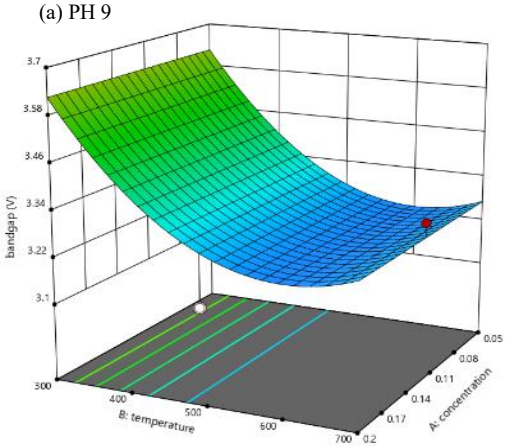

(b) PH 10

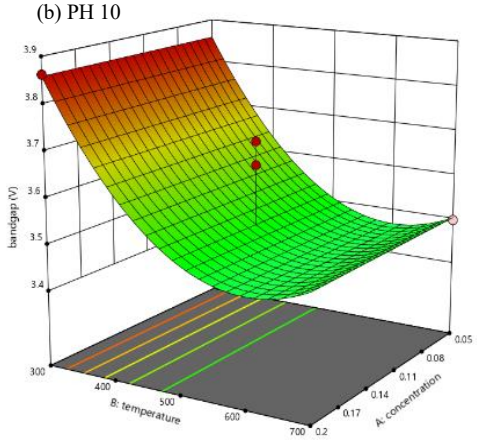

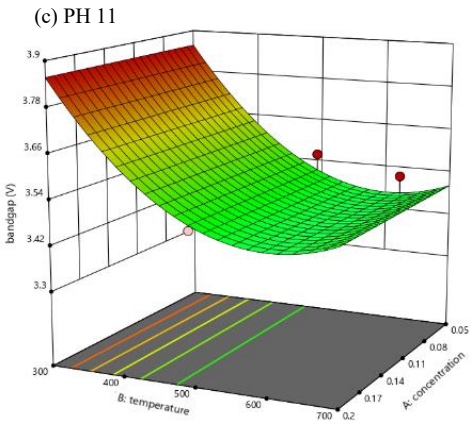

Fig. 5. 3D surface plot between bandgap versus temperature versus concentration for (a) pH 9, (b) pH 10 and (c) pH 11.

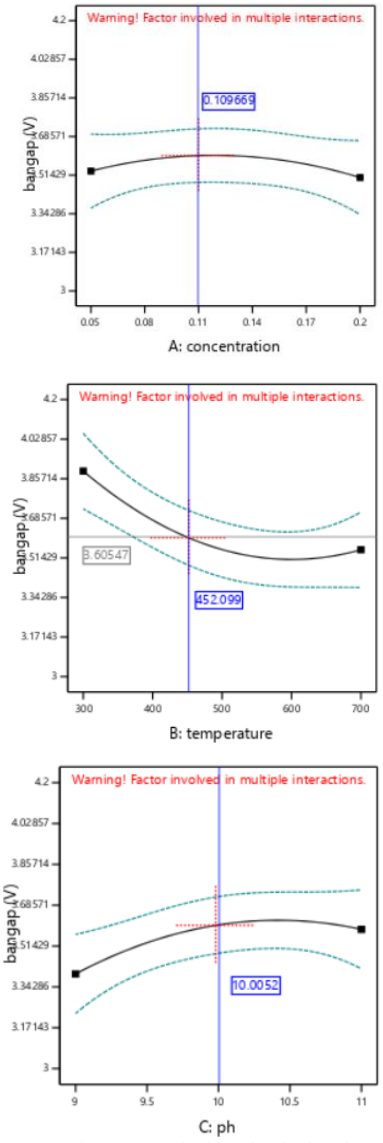

Fig. 6. Perturbation plot for bandgap.

Figure 6 illustrates the perturbation plots for bandgap variation as a function of concentration (A), annealing temperature (B), and pH (C). Notably, the bandgap exhibits a slight downward curvature with increasing temperature and concentration. At the same time, it shows a mild upward trend with increasing pH up to around 10, beyond which it does not change. This trend implies that increasing pH enhances the optical bandgap until a critical threshold is reached, potentially due to changes in film stoichiometry or defect density.

The contour plot in Fig. 7 reveals that the maximum bandgap energy of 3.6 eV is observed under synthesis conditions of low annealing temperature (300–400ºC) and high precursor pH (10.5–11), with the precursor concentration fixed at 0.125 M. At low annealing temperatures, the material's crystalline phase is preserved, while excessive defect formation is minimized. Additionally, a high pH likely enhances the hydrolysis and condensation processes in the sol-gel synthesis, promoting the formation of uniform and chemically stable NiO with reduced defect density [18].

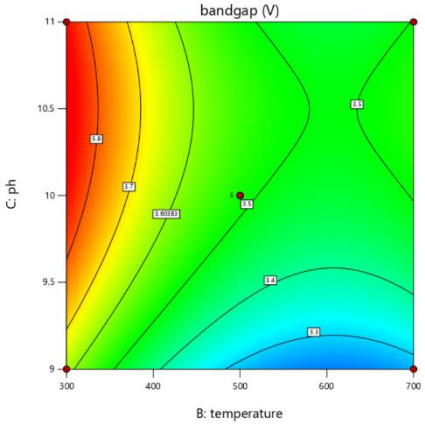

Fig. 7. Contour plot for concentration fixed at 0.125M.

R-squared value of 0.75 implies that 75% of the variance in the dependent variable, that is, bandgap, can be explained by the independent variable(s), that is, temperature (B) and pH(C) in the model. Based on regression analysis, the quadratic model equations for the two responses, temperature (B and pH(C), in terms of actual values, can be written by considering the significant terms as follows:

$$\text{Bandgap} = 3.52 - 0.1773B + 0.1154C + 0.1651B^2 - 0.1166C^2$$

E. The Influence of All Parameters on Resistance

The second response analysed in this study was the electrical resistance of NiO thin films. In Design Expert software, ANOVA results for electrical resistance shown in Table V. Among all parameters, annealing temperature (B) was found to be the most significant factor influencing resistance, with a p-value less than 0.0001. Nickel acetate tetrahydrate concentration (A) also showed a statistically significant effect (p = 0.0010), while solution pH (C) has a moderate impact (p = 0.0110). The P value indicates that higher temperature and optimized concentration levels strongly affect the carrier transport behaviour in the NiO films. These findings demonstrate that annealing temperature plays a critical

role in tuning the electrical resistance of NiO, possibly by improving crystallinity and reducing grain boundary scattering. Samples annealed at higher temperatures exhibited larger crystallite sizes than those annealed at lower temperatures. The statistical analysis (ANOVA) confirmed annealing temperature as the dominant factor affecting resistance ($p < 0.0001$), aligning with the observed trend that higher temperature promotes grain growth and structural ordering.

Table V. Anova result for resistance.

Source	p-value	Remark
Model	< 0.0001	significant (p<0.05)
A-concentration	0.001	significant (p<0.05)
B-temperature	< 0.0001	significant (p<0.05)
C-ph	0.011	significant (p<0.05)

As shown in the perturbation plot in Fig. 8, the response curve for temperature (B) exhibits a pronounced curvature, indicating a strong nonlinear relationship with resistance. This observation is consistent with the ANOVA results. The plot reveals that resistance decreases initially with increasing temperature, reaching a minimum near 400ºC, beyond which it sharply increases, highlighting the presence of an optimal temperature for minimizing resistance. In contrast, the perturbation curves for concentration and pH are relatively flat, suggesting that their effects on resistance are comparatively less significant within the tested range. These findings align with the statistical analysis, where concentration (A) and pH (C) had moderate significance ($p = 0.0010$ and $p = 0.0110$, respectively), but did not exhibit strong curvature or interaction effects.

The contour in Fig. 9 represents the variation in resistance, with red regions indicating high resistance and blue regions representing low resistance, depending on the precursor concentration (A) versus annealing temperature (B) versus pH (C). In the first plot (A vs. C), resistance is lowest at moderate precursor concentrations and pH values, as indicated by the central blue region. The extreme values of either parameter lead to higher resistance (red areas). The second plot (A vs. B) demonstrates that resistance increases as annealing temperature increases, particularly at lower precursor concentrations, with blue regions forming at temperatures above 500ºC. The third plot (B vs. C) shows that resistance is mainly influenced by annealing temperature, with a clear growth in resistance as temperature increases, regardless of pH. These findings highlight the significant impact of annealing temperature and the interplay between precursor concentration and pH in minimizing resistance.

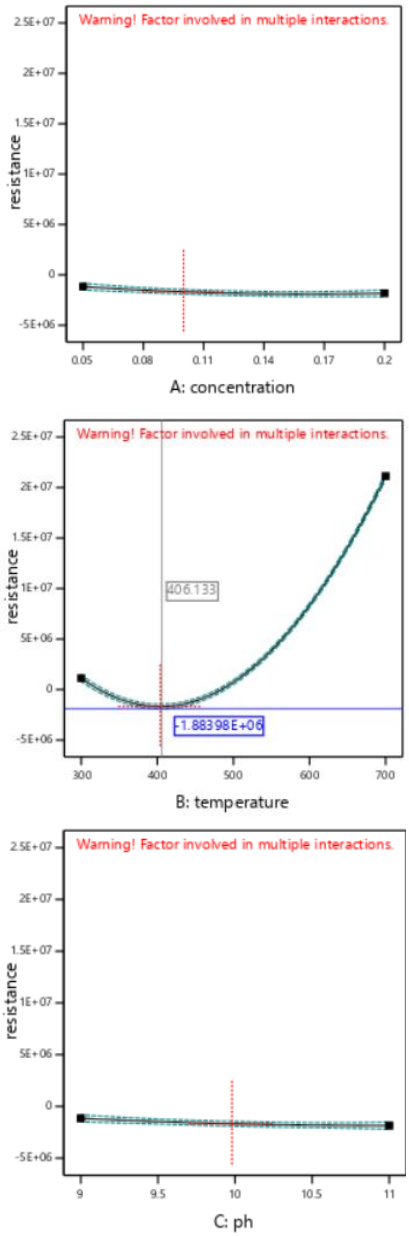

Fig. 8. Perturbation plot to get the lowest resistance.

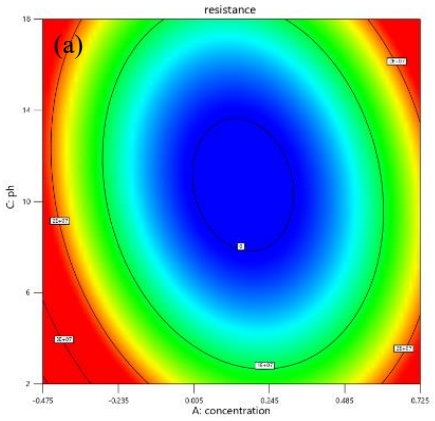

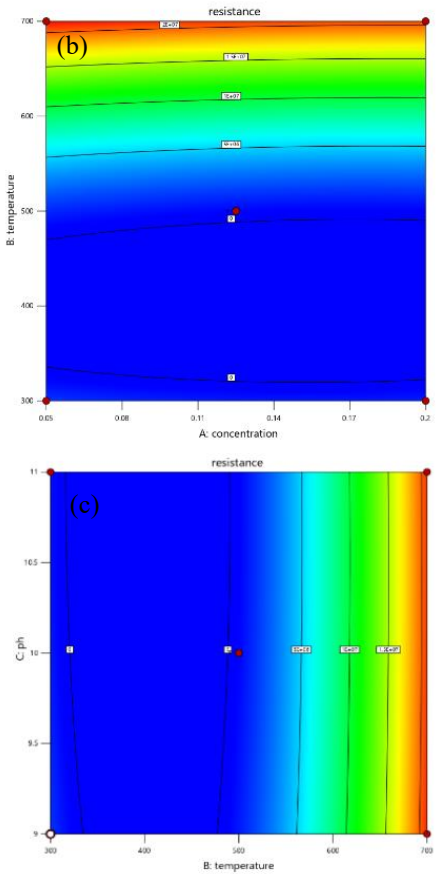

Fig. 9. Resistance contour plot (a) pH versus concentration, (b) temperature versus concentration and (c) temperature versus pH.

R-squared value of 0.99 implies that 99% of the variance in the dependent variable, that is, resistance, can be explained by the independent variables (s) that are concentration (A), temperature (B), and pH (C) in the model. Based on regression analysis, the quadratic model equations for the three responses, precursor concentration (A), temperature (B), and pH(C), in terms of actual values, can be written by considering the significant terms as follows:

$$\text{Resistance} = 542{,}800 + -421{,}125A + 9.9395E{+}06B + -267{,}375C + -188{,}000AB + 71{,}250AC + 127{,}000BC + 330{,}975A^2 + 1.04047E{+}07B^2 + 179{,}975C^2$$

F. The Influence of All Parameters on The Bandgap and Resistance

Figure 10 illustrates the correlation between optical bandgap, crystallite size, and electrical resistance for seven selected NiO thin film samples synthesized under varying precursor concentrations, pH levels, and annealing temperatures. As for the same pH but different annealing temperature, the decrease in bandgap with annealing temperature could be due to an increase in crystalline size and reduction of defect sites. According to XRD results, the crystalline size has increased with increased annealing temperature. As the grain size has increased, the grain boundary density of a film decreased; subsequently, the scattering of carriers at grain boundaries has reduced. At 300ºC, the higher pH promotes larger crystallite sizes and improved crystallinity, reducing resistance by enabling more efficient charge transport. At 700ºC, the combined effects of higher temperature and pH reduce oxygen vacancies and decrease crystallite size, increasing resistance due to reduced carrier concentration and more significant grain boundary effects [19]. The resistance of NiO decreases with better crystallinity and larger crystallite sizes at low temperatures and higher pH. In contrast, at higher temperatures and pH, resistance increases due to the reduction of oxygen vacancies and the dominance of grain boundary effects. The predicted optimum (0.125 M precursor concentration, pH 10, and annealing temperature of 450 °C) was validated experimentally. This correlation demonstrates that BBD effectively captures nonlinear interactions among synthesis parameters and provides reliable guidance for fabricating sol–gel NiO thin films with targeted properties.

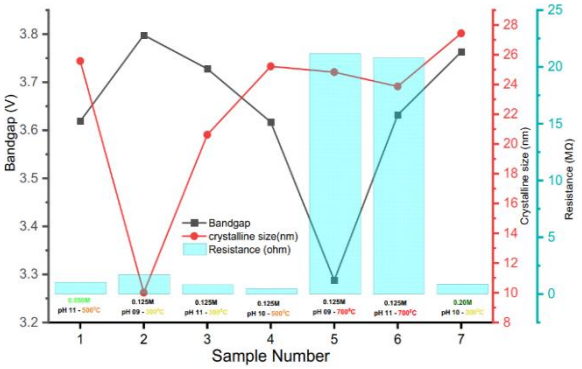

Fig. 10. Influence of all parameters on bandgap and resistance.

IV. CONCLUSION

This study successfully demonstrates the use of Response Surface Methodology (RSM) to optimize the sol-gel synthesis of NiO thin films for application as hole transport layers in perovskite solar cells. Among the parameters studied, annealing temperature and pH exhibited the most significant influence on both the optical bandgap and electrical resistance, while precursor concentration showed a lesser effect. The optimal synthesis condition identified at 0.125 M precursor concentration, pH 10, and 450 °C annealing temperature produced a NiO film with a bandgap of 3.6 eV and low electrical resistance, favourable for efficient hole transport and minimal recombination. The findings highlight the crucial interplay between process parameters in tuning material properties and provide insights for achieving targeted performance through statistically guided synthesis. Future work should investigate the long-term stability and photovoltaic performance of these films in full perovskite device stacks.

ACKNOWLEDGEMENT

The authors thank to Universiti Putra Malaysia (UPM) and Universiti Teknikal Malaysia Melaka (UTeM) for technical support and facilities. This work was financially supported by Universiti Putra Malaysia (UPM).

FUNDING STATEMENT

The authors received funding from Universiti Putra Malaysia (UPM) for the research.

AUTHOR CONTRIBUTIONS

Nurbahirah Norddin: Experimental Design, Methodology, Investigation, and Data Analysis. Suhaidi Shafie: Review, Manuscript Refinement, and Supervision. Muhammad Idzdihar Idris: Resources and Technical Guidance.
Xinzhi Liu and Ismail Lawal: Data Analysis and Editing. Mohd Nizar Hamidon: Resources and Technical Guidance.

CONFLICT OF INTERESTS

No conflict of interests was disclosed.

ETHICS STATEMENTS

Our publication ethics follow The Committee of Publication Ethics (COPE) guideline. https://publicationethics.org/

REFERENCES

[1] A. C. Nkele *et al*., "The Use of Nickel Oxide As A Hole Transport Material in Perovskite Solar Cell Configuration: Achieving A High Performance and Stable Device," *Int. J. Ener. Res.*, vol. 44, no. 13, pp. 9839–9863, 2020.

[2] S. Sajid, S. Alzahmi, I. B. Salem and I. M. Obaidat, "Guidelines for Fabricating Highly Efficient Perovskite Solar Cells with Cu_2O As the Hole Transport Material," *Nanomater.*, vol. 12, no. 19, pp. 3315, 2022.

[3] A. Hassan *et al*., "Recent Defect Passivation Drifts and Role of Additive Engineering in Perovskite Photovoltaics," *Nano Ener.*, vol. 101, pp. 107579, 2022.

[4] K. M. Reza *et al.*, "Tailored PEDOT:PSS Hole Transport Layer for Higher Performance in Perovskite Solar Cells: Enhancement of Electrical and Optical Properties with Improved Morphology," *J. Ener. Chem.*, vol. 44, pp. 41–50, 2020.

[5] S. D. Dhas, P. S. Maldar, M. D. Patil, M. R. Waikar, R. G. Sonkawade and A. V. Moholkar.,"Sol-gel Synthesized Nickel Oxide Nanostructures on Nickel Foam and Nickel Mesh for A Targeted Energy Storage Application," *J. Ener. Stor.*, vol. 47, pp. 103658, 2022.

[6] J. Sun *et al.,* "NiO_x-Seeded Self-Assembled Monolayers As Highly Hole-Selective Passivating Contacts for Efficient Inverted Perovskite Solar Cells," *Solar RRL*, vol. 5, no. 11, pp. 2100663, 2021.

[7] Z. Jin *et al.,* "Modification of NiO(x) Hole Transport Layer for Acceleration of Charge Extraction in Inverted Perovskite Solar Cells," *RSC Adv.*, vol. 10, no. 21, pp. 12289–12296, 2020.

[8] S. I. S. Shaharuddin *et al*., "Effect of Spinning Parameters on PLA/PPC/curcumin Microfiber Diameter: An Investigation via Response Surface Methodology," *IIUM Eng. J.*, vol. 21, no. 2, pp. 197–211, 2020.

[9] N. Kumari, S. R. Patel and J. V. Gohel, "Superior Efficiency Achievement for Fapbi3-Perovskite Thin Film Solar Cell by Optimization with Response Surface Methodology Technique and Partial Replacement of Pb by Sn," *Optik*, vol. 176, pp. 262–277, 2019.

[10] K. Ghorui, R. Sarkarand and B. Tudu., "Effect of Precursor Concentration on Structural and Optical Properties of Nickel Oxide Nanoparticles Synthesized by Facile Sol-gel Method," *Mater. Today: Proc.*, vol. 103, pp. 210-214, 2024.

[11] R. G. Larson, and T. J. Rehg., "Spin Coating BT - Liquid Film Coating: Scientific Principles and Their Technological Implications," *Dordrecht: Springer Netherlands*, pp. 709–734, 1997.

[12] S. T. Akinkuade, W. E. Meyer and J. M. Nel, "Effects of Thermal Treatment on Structural, Optical and Electrical Properties of NiO Thin Films," *Phys. B: Cond. Mat.*, vol. 575, pp. 411694, 2019.

[13] H. Bao *et al.*, "Samarium-Doped Nickel Oxide for Superior Inverted Perovskite Solar Cells: Insight into Doping Effect for Electronic Applications," *Adv. Funct. Mater.*, vol. 31, no. 34, pp. 2102452, 2021

[14] J. Zhou *et* al., "Highly Efficient and Stable Perovskite Solar Cells via A Multifunctional Hole Transporting Material," *Joule*, vol. 8, no. 6, pp. 1691–1706, 2024.

[15] M. Vidhya, *et al*, "Effect of Molar Concentration on Optoelectronic Properties of NiO Nanoparticles for P-N Junction Diode Application," *Sens. and Act. A: Phys.*, vol. 366, pp. 114995, 2024.

[16] X. Cai *et* al., "A Review for Nickel Oxide Hole Transport Layer and Its Application in Halide Perovskite Solar Cells, *Mater. Today Sustain.*, vol. 23, pp. 100438, 2023.

[17] M. Ba-Abbad, P. V. Chai, M.S . Takriff, A. Benamor and A. W. Mohammad, "Optimization of Nickel Oxide Nanoparticle Synthesis Through The Sol–gel Method using Box–Behnken Design," *Mater. & Desig.*, vol. 86, pp. 948–956, 2015.

[18] S. Muniandy, M. I. Idris, Z. A. F. Napiah, N. S. T. Kie, Z. Baharudin and M. Rashid., "Influence of pH-Driven Synthesis on The Performance of NiO As A Hole Transport Layer in Perovskite Solar Cells, *Eng. J.*, vol. 29, no. 4, pp. 23–37, 2025.

[19] M. Shi, *et al*., "Temperature-Controlled Crystal Size of Wide Band Gap Nickel Oxide and Its Application in Electrochromism," *Micromachin.,* vol. 12, no. 1, pp. 80, 2021.